

RESEARCH ARTICLE | SEPTEMBER 10 2020

Bioelectronic control of chloride ions and concentration with Ag/AgCl contacts

Special Collection: [Advances in Bioelectronics: Materials, Devices, and Translational Applications](#)

Manping Jia ; Harika Dechiruji ; John Selberg ; Pattawong Pansodtee ; Juanita Mathews; Chunxiao Wu; Michael Levin; Mircea Teodorescu; Marco Rolandi  



APL Mater. 8, 091106 (2020)

<https://doi.org/10.1063/5.0013867>

 CHORUS



Articles You May Be Interested In

A multi-ion electrophoretic pump for simultaneous on-chip delivery of H^+ , Na^+ , and Cl^-


APL Mater. (April 2022)

On-chip on-demand delivery of K^+ for *in vitro* bioelectronics

AIP Advances (December 2022)

Graphene nanostructures for input–output bioelectronics

Biophysics Rev. (December 2021)



Your One-Stop Shop for the Best Brands in Optics

- Extensive inventory with over 34,000 products available & 2,900 new products
- Fast shipping from our 9 distribution centres around the globe
- Bringing 80+ years of optical expertise to customers worldwide

Edmund
optics | worldwide

[Shop Now](#)






Bioelectronic control of chloride ions and concentration with Ag/AgCl contacts

Cite as: APL Mater. 8, 091106 (2020); doi: 10.1063/5.0013867

Submitted: 14 May 2020 • Accepted: 7 August 2020 •

Published Online: 10 September 2020



Manping Jia,¹  Harika Dechiruji,¹  John Selberg,¹  Pattawong Pansodtee,¹  Juanita Mathews,² Chunxiao Wu,¹ Michael Levin,² Mircea Teodorescu,¹ and Marco Rolandi^{1,a)} 

AFFILIATIONS

¹Department of Electrical and Computer Engineering, University of California Santa Cruz, Santa Cruz, California 95064, USA

²Allen Discovery Center at Tufts University, Medford, Massachusetts 02155, USA and Wyss Institute for Biologically Inspired Engineering, Harvard University, Boston, Massachusetts 02155, USA

Note: This paper is part of the Special Topic on Advances in Bioelectronics.

a) Author to whom correspondence should be addressed: mrolandi@ucsc.edu

ABSTRACT

Translation between ionic currents and measurable electronic signals is essential for the integration of natural systems and artificial bioelectronic devices. Chloride ions (Cl^-) play a pivotal role in bioelectricity, and they are involved in several brain pathologies, including epilepsy and disorders of the autistic spectra, as well as cancer and birth defects. As such, controlling $[\text{Cl}^-]$ in solution can actively influence biochemical processes and can be used in bioelectronic therapies. Here, we demonstrate a bioelectronic device that uses Ag/AgCl contacts to control $[\text{Cl}^-]$ in solution by electronic means. We do so by exploiting the potential dependence of the reversible reaction, $\text{Ag} + \text{Cl}^- \leftrightarrow \text{AgCl} + \text{e}^-$, at the contact/solution interface, which is at the basis of the well-known Ag/AgCl reference electrode. In short, a negative potential on the Ag/AgCl contact transfers Cl^- from the contact to the solution with increasing $[\text{Cl}^-]$ and vice versa. With this strategy, we demonstrate precise spatiotemporal control of $[\text{Cl}^-]$ in solution that can be used to affect physiological processes that are dependent on $[\text{Cl}^-]$. As proof-of-concept, we use $[\text{Cl}^-]$ control to influence the membrane voltage on human pluripotent stem cells.

© 2020 Author(s). All article content, except where otherwise noted, is licensed under a Creative Commons Attribution (CC BY) license (<http://creativecommons.org/licenses/by/4.0/>). <https://doi.org/10.1063/5.0013867>

I. INTRODUCTION

Ranging from intercellular communication to organ function, ionic species play an important role in natural systems.¹ A majority of physiological processes, such as muscle contraction, neuronal signaling, and metabolism, involve the exchange of ions between cells.² On the other hand, electrons and holes dominate communication between electronic devices. Bioelectronics bridges natural systems and electronic devices by translating ionic signals in the body into electronic signals for sensing and control.^{3–7} Iontronic devices, for example, address individual ions and small molecules to control specific physiological pathways.^{4,8,9} These include the precise delivery of Ca^{2+} , K^+ , and gamma-aminobutyric acid (GABA) to control epileptiform activities and treat neuropathic pain with low dosage and less side effect.^{10,11} To this end, our group has demonstrated the control of H^+ in field-effect transistors¹² and memories,¹³ enzymatic logic gates and bioluminescence,¹⁴ ion channel devices,^{15–18} H^+

modulators for delivery of cargo^{19,20} and glucose sensing.²⁰ These devices are enabled by using Pd/PdH_x contacts, also known in the reversible H reference electrode, to translate electronic signals into H^+ signals. This translation occurs according to the potential dependent reversible reduction, $\text{H}^+ + \text{e}^- \leftrightarrow \text{H}$, at the Pd/PdH_x-solution interface and the subsequent physisorption of H onto Pd to form PdH_x.²¹ An electrical potential applied on the Pd/PdH_x contact shifts the reaction equilibrium and induces the transfer of H^+ to and from the solution, which effectively controls $[\text{H}^+]$ in the solution. Cl^- is a major anion in the physiological environment and functions importantly in many fundamental biological processes, including the regulation of intracellular pH gradients, maintenance of intracellular volume, and resting membrane potential.^{22–25} Controlling $[\text{Cl}^-]$ in solution has great significance in regulating extra- and intracellular distribution of chloride, which influences cell growth and differentiation, metastatic conversion, patterning of innervation, and neuronal excitability in the central nervous system.^{25–28}

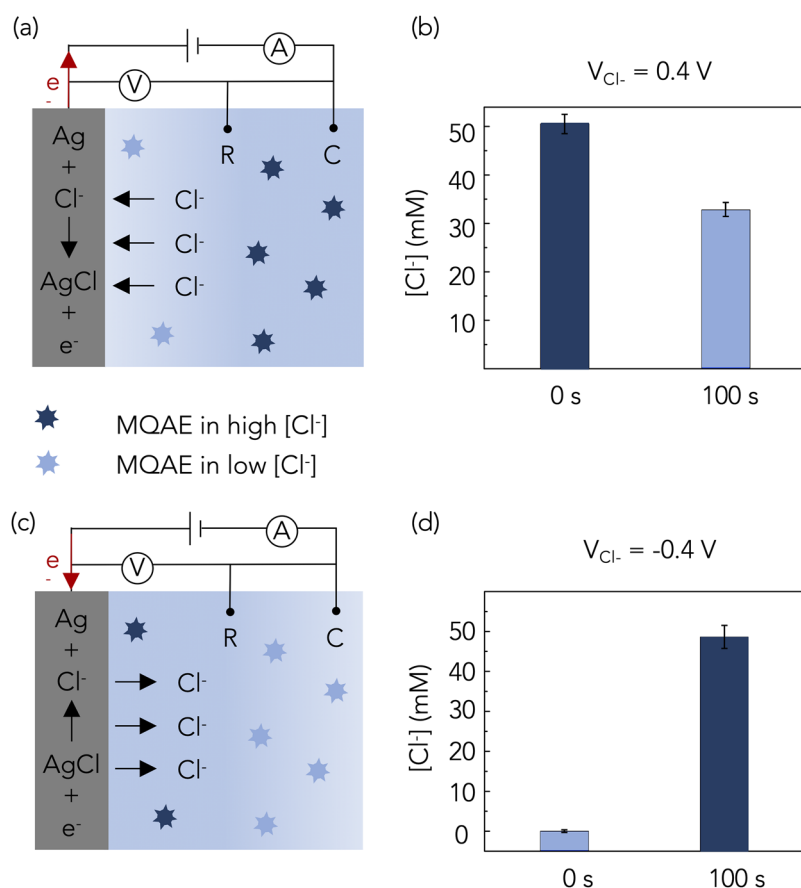
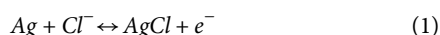


FIG. 1. Schematic of the prototype chloride transducer and working mechanism. This setup has a standard three-electrode configuration. MQAE is a fluorescence dye monitoring $[\text{Cl}^-]$ change in solution, whose intensity increases with lower $[\text{Cl}^-]$. (a) Anodic voltage transfers Cl^- from solution into the Ag/AgCl contact, which decreases $[\text{Cl}^-]$ and brightens MQAE. (b) $[\text{Cl}^-]$ changes from 50 mM to 32 mM by applying 0.4 V for 100 s. (c) Cathodic voltage transfers Cl^- from the Ag/AgCl contact into solution, thus increasing $[\text{Cl}^-]$ and quenching MQAE. (d) $[\text{Cl}^-]$ changes from 0 mM to 48 mM by applying -0.4 V for 100 s.

Here, we control $[\text{Cl}^-]$ in solution by exploiting perhaps the best-known reference electrode, Ag/AgCl.^{23,29–32} We do so by driving the reaction



out of equilibrium condition with a potential (V_{Cl^-}) on the Ag/AgCl contact to effectively transfer Cl^- across the contact/solution interface (Fig. 1). While Ag/AgCl is a well-known system, the use of Ag/AgCl to control $[\text{Cl}^-]$ as an e^- to Cl^- transducer has yet to be reported to the best of our knowledge. Furthermore, we adapt Ag/AgCl contact to a bioelectronic device, a chloride modulator with a chloride reservoir, and a target chamber that is able to host cells. We use this chloride modulator to demonstrate the proof-of-concept actuation of membrane voltage (V_{mem}) on human pluripotent stem cells (hiPSCs).

II. Cl^- TO ELECTRON TRANSDUCER

First, we use an Ag/AgCl wire as a chloride transducer to show the ability of Ag/AgCl to control $[\text{Cl}^-]$ in solution. We do so in a standard three-electrode configuration with the Ag/AgCl wire as the working electrode (W), glass Ag/AgCl as the reference electrode (R), and platinum (Pt) wire as the counter electrode (C). Figure 1(a) describes how an anodic voltage, V_{Cl^-} , transfers Cl^- from solution to the Ag/AgCl wire according to $\text{Ag} + \text{Cl}^- \rightarrow \text{AgCl} + e^-$ and, thus, reduces $[\text{Cl}^-]$. The excess e^- flows out of the Ag/AgCl

contact into the lead. We use (*N*-(ethoxycarbonylmethyl)-6-methoxyquinolinium bromide) (MQAE) to monitor $[\text{Cl}^-]$. MQAE is a diffusion-limited collisional Cl^- -quenched fluorescent dye whose intensity decreases when $[\text{Cl}^-]$ increases. We calibrate MQAE using the Stern–Volmer equation (Fig. S1) and quantify $[\text{Cl}^-]$.³³ Figure 1(b) shows $[\text{Cl}^-]$ decreases from 50 mM to 32 mM when $V_{\text{Cl}^-} = 0.4 \text{ V}$ for 100 s. Figure 1(c) describes how a cathodic voltage, V_{Cl^-} , transfers Cl^- from the Ag/AgCl wire to the solution according to $\text{AgCl} + e^- \rightarrow \text{Ag} + \text{Cl}^-$ and, thus, increases $[\text{Cl}^-]$. Figure 1(d) shows that $[\text{Cl}^-]$ increases from 0 mM to 48 mM when $V_{\text{Cl}^-} = -0.4 \text{ V}$ for 100 s. These ranges and changes for $[\text{Cl}^-]$ are comparable to changes in $[\text{Cl}^-]$ plasma, interstitial fluids, and intracellular fluids,²² and they are, thus, relevant for biological applications.

One of the advantages of using AgCl to transfer Cl^- to and from solution is the fact that AgCl is selective to Cl^- and is able to affect $[\text{Cl}^-]$ under physiological conditions with little to no interference from other ions. To this end, we demonstrate that the Cl^- transducer works in a complex solution such as stem cell culture media (NeurobasalTM-A Medium, ThermoFisher) that contains 79.6 mM NaCl, 26 mM NaHCO_3 , and 0.9 mM KH_2PO_4 . With $V_{\text{Cl}^-} = 0.6 \text{ V}$ for 100 s, we are still able to remove Cl^- from solution and reduce $[\text{Cl}^-]$ from 79.6 mM to $47 \pm 2 \text{ mM}$. Repeating the experiment without HCO_3^- and H_2PO_4^- ions leads to the same result with the final $[\text{Cl}^-] = 46 \pm 5 \text{ mM}$ (Fig. S2). While we are not able to monitor the change in concentration of the other anions, these

results indicate that the presence of other anions does not affect the Cl^- transducer indicating that AgCl is indeed specific to Cl^- . From our work with the AgCl wire, we found that transferring Cl^- from the Ag/AgCl contact into the solution is more efficient than transferring Cl^- from the solution to the contact. One of the reasons can be that when applying an anodic voltage, Cl^- ions are absorbed into Ag/AgCl electrodes immediately, and a depletion area forms around the electrodes.³⁴ Then, the reaction is limited by Cl^- migration to the contact/solution interface. We further investigate the electrode kinetics of Ag/AgCl conversion in Sec. III to verify the hypothesis.

III. KINETICS OF THE CONVERSION BETWEEN Ag AND AgCl

To better understand and optimize the Cl^- transducer, we investigate the kinetics of Cl^- transfer at different potentials. Surprisingly, not many investigations on the kinetics of the conversion between Ag/AgCl under dynamic polarization or under other non-equilibrium exist.³⁵ For a Ag/AgCl electrode in solution containing Cl^- , the Cl^- in the AgCl are in equilibrium with the $[\text{Cl}^-]$ in solution. As such, a Ag/AgCl contact shows a lower electrode potential in a solution with higher $[\text{Cl}^-]$ and vice versa.²³ The well-known Ag/AgCl reference electrode takes advantage of this relationship by reading a constant potential when encapsulated in an internal electrolyte with a constant $[\text{Cl}^-]$.³⁶ AgCl has been used as the gate electrode in organic electrochemical transistors (OECTs), which utilized its faradaic reactions in halide electrolytes to achieve higher current modulation compared to Pt electrodes.³⁷ However, there are few studies exploring the dynamic change in the Ag/AgCl system. Little is known about the kinetics of the conversion between Ag and AgCl.^{35,38} Although people have reported the open circuit potential (OCP) and cyclic voltammetry (CV) of Ag/AgCl, the analysis of the conversion between e^- and Cl^- is absent. Here, we explore the kinetics of Ag/AgCl conversion of miniaturized on-chip Ag/AgCl nanoparticle (NP) electrodes. We use Ag/AgCl NPs to create an

interface with a higher surface area and capacitance for better conversion efficiency.³⁹ The conversion between Ag/AgCl under non-equilibrium conditions is consistent with Cl^-/e^- transformation, which is critical for controlling $[\text{Cl}^-]$ by electronic means.

We electroplate Ag NPs on thin-film Au contacts and chlorinate the Ag NPs into Ag/AgCl NPs in a 50 mM KCl solution (Fig. S3). The bare Ag/AgCl NP electrode we make here is a “quasi-reference electrode,” whose electrical potential depends on $[\text{Cl}^-]$ in solution according to the thermodynamically based Nernst relationship,

$$V_{\text{Cl}^-} = V_{\text{Cl}^-}^0 - 0.059 \lg[\text{Cl}^-], \quad (2)$$

where $V_{\text{Cl}^-}^0$ is the standard potential of Ag/AgCl.

Ag/AgCl conversion depends on $[\text{Cl}^-]$ in solution and the applied potential (V_{Cl^-}). Here, we record the open circuit potential (V_{OCP}) of Ag/AgCl contact in various $[\text{Cl}^-]$ solutions under equilibrium conditions with a three-electrode configuration at room temperature. Figure 2(a) shows the V_{OCP} of Ag/AgCl in 1 mM, 10 mM, 100 mM, and 1M KCl, respectively. V_{OCP} and logarithmic scale of $[\text{Cl}^-]$ shows a linear relationship with a slope of -55.35 mV and $R^2 = 0.999$, as expected from the Nernst equation. We use the values of V_{OCP} to define the process map for the Cl^- transducer as a function of $[\text{Cl}^-]$ and V_{Cl^-} [Fig. 2(a)]. The straight line in the graphs joins the V_{OCP} s at different $[\text{Cl}^-]$ ions and represents equilibrium (as many Cl^- transfer from the solution into the electrode as they transfer from the electrode into the solution). This line also marks the threshold of the Ag/AgCl conversion. For a combination of V_{Cl^-} and $[\text{Cl}^-]$ in the gray area below the line, Cl^- transfer into the solution increasing $[\text{Cl}^-]$ and for a combination of V_{Cl^-} and $[\text{Cl}^-]$ above the line in the white area Cl^- transfer from the solution decreasing $[\text{Cl}^-]$.

To further study the electrode kinetics at the interface of the Ag/AgCl contact and solution, we investigate the limiting mechanism of this electrochemical reaction [Fig. 2(b)]. In detail, we cycle the voltage of Ag/AgCl NP electrodes between -0.8 V and 0.8 V vs a glass Ag/AgCl electrode. Pt wire is the counter electrode as usual. We

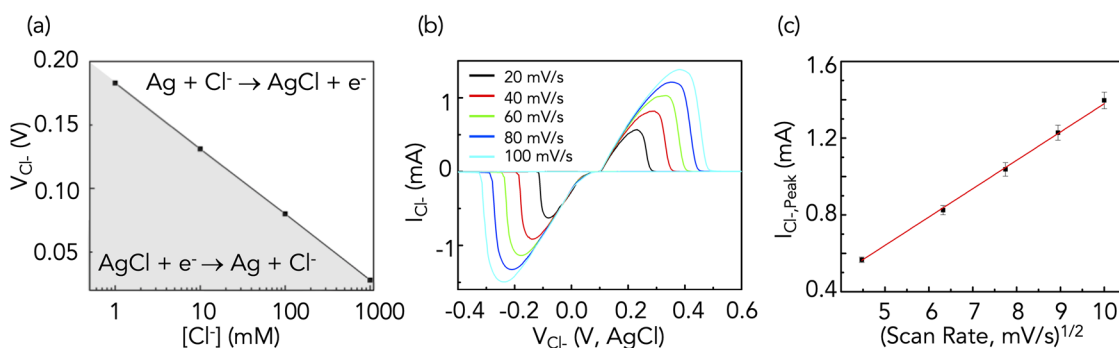


FIG. 2. Kinetics of the conversion between Ag/AgCl. (a) The linear relationship between V_{OCP} and logarithmic scale of $[\text{Cl}^-]$ represents equilibrium as well as the threshold of Ag/AgCl conversion. In the white area above the line, $\text{Ag} + \text{e}^- \rightarrow \text{AgCl}$; in the gray area under the line, $\text{AgCl} + \text{e}^- \leftarrow \text{Ag} + \text{Cl}^-$. (b) CV of Ag/AgCl electrodes with a series of scan rates, 20 mV/s, 40 mV/s, 60 mV/s, 80 mV/s, and 100 mV/s. The redox peaks show that the reaction is electron transfer dominated, and the current increases at a higher scan rate due to the reduced diffusion layer. (c) Relationship of the anodic peak current of Ag/AgCl ($I_{\text{Cl}^-, \text{Peak}}$) vs the square root of the scan rate in CV measurements. The excellent linear relationship shows that the reaction is limited by the diffusion of Cl^- to the electrode following Randles-Sevcik equation. The standard error is derived from three electrodes.

use a series of scan rates, 20 mV/s, 40 mV/s, 60 mV/s, 80 mV/s, and 100 mV/s, respectively. Taking 40 mV/s as an example, the interfacial reaction can be explained as below. During the scan of V_{Cl^-} from 0 V to 0.8 V, Cl^- is absorbed onto Ag/AgCl and oxidizes Ag to AgCl. I_{Cl^-} increases to a peak with higher V_{Cl^-} and then becomes smaller by the delivery of Cl^- from the bulk solution. Thus, the mass

transport of Cl^- becomes the limitation of the electrochemical reaction, and the current decays gradually.⁴⁰ After the scan direction is switched to negative, V_{Cl^-} is still sufficiently positive to oxidize Ag, so I_{Cl^-} continues until V_{Cl^-} becomes strong enough to reduce AgCl. Then, Cl^- starts to be released from the electrode, reaches a cathodic peak and decays as AgCl is consumed. With the increase

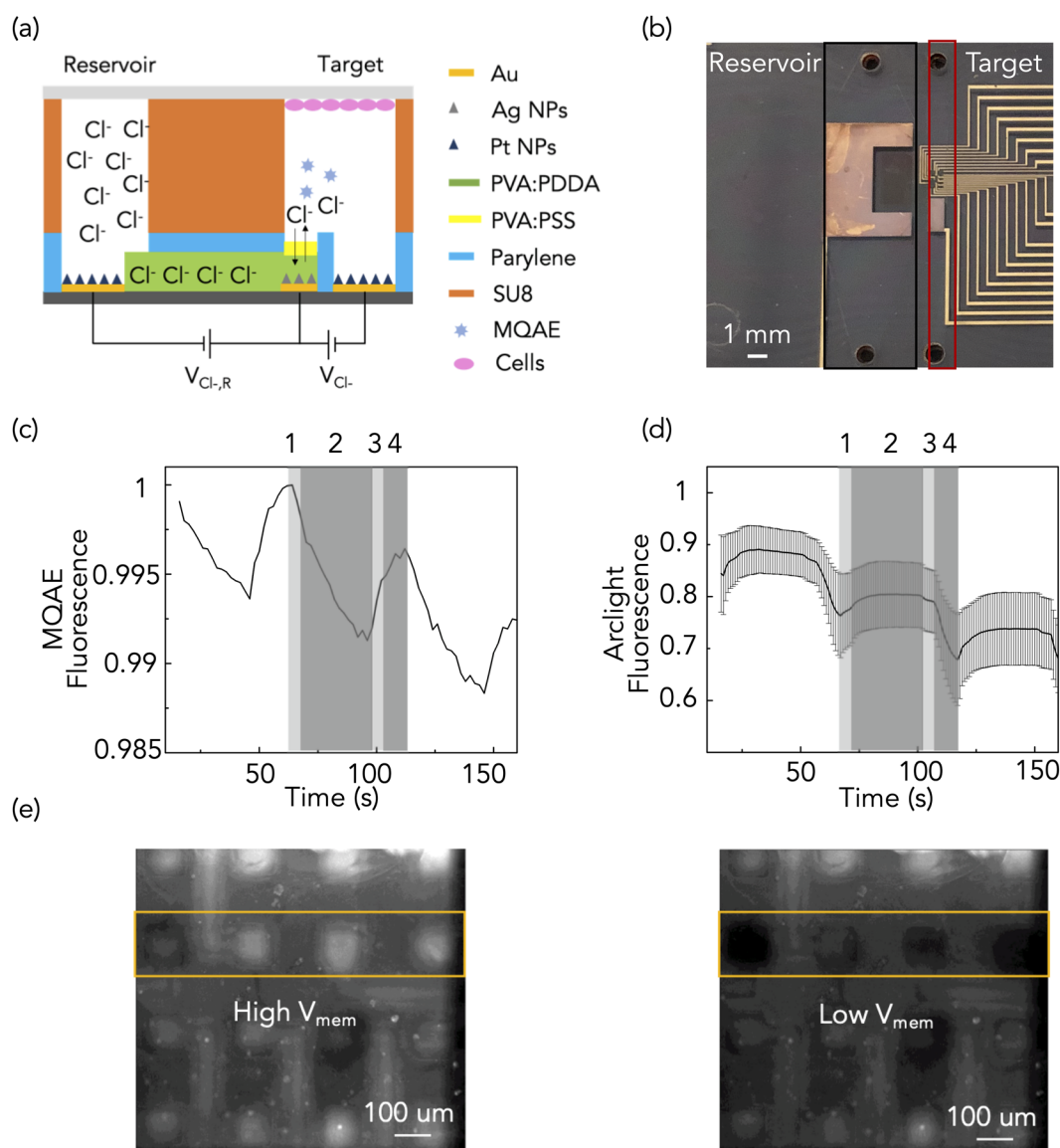


FIG. 3. Chloride modulator. (a) Schematic of the chloride modulator (side view) and operating principle. Reservoir and target are connected by using an anion exchange membrane (AEM) in which Cl^- are driven by V_{Cl^-} . Reservoir has a high $[\text{Cl}^-]$ solution providing the Cl^- source, and $[\text{Cl}^-]$ in target is under control. (b) Optical image of the chloride modulator. The reservoir (black line) and target (red line) are separated by SU eight microfluidic channels and the holes on the glass slide provide the inlet and outlet. (c) $[\text{Cl}^-]$ change results from the 4-step process in Table I for three cycles, which is indicated by the MQAE fluorescence intensity. Temporal change corresponding to each step is shown with different colors in the second cycle as a representation. (d) V_{mem} change in cells resulting from the same operation is indicated by the ArcLight fluorescence intensity. The data come from three devices. (e) Fluorescence images of the cells over MEAs with high V_{mem} (t = 75 s) and low V_{mem} (t = 119 s). The highlighted row is under operation.

in the scan rate, the diffusion layer becomes smaller, and it takes less time to record one cycle, inducing I_{Cl^-} increase.^{41,42} The measured current in CV with a redox couple is mainly faradaic current, which is from the charge transfer at the interface of the electrode contact/solution and depends on the kinetics of charge transfer at the surface and the redox species diffusion to the surface.⁴¹ We plot the peak currents ($I_{Cl^-,Peak}$) of CV vs the square root of scan rates of three electrodes in Fig. S4, which all show an extraordinary proportional relationship, and the standard error is shown in Fig. 2(c). According to the Randles-Sevcik equation [Eq. (2)], the analytes, Cl^- , are not adsorbed on the electrode but freely diffused in the solution. Thus, we conclude that Ag/AgCl conversion is a Cl^- -diffusion controlled reversible electrochemical reaction,⁴⁰

$$I_{Cl^-,Peak} = 0.4463nFAC\left(\frac{nFvD}{RT}\right)^{\frac{1}{2}}, \quad (3)$$

where $I_{Cl^-,Peak}$, R , F , and T are peak current of cathodic or anodic reaction, gas constant, Faraday constant, and absolute temperature, respectively. A , C , D , and v are electrode area, concentration of the analyte, diffusion coefficient, and scan rate of CV.

IV. CHLORIDE MODULATOR WITH CELLS

As the translation between Cl^- and e^- is in parallel with the conversion between Ag/AgCl, which depends on V_{Cl^-} and $[Cl^-]$ in solution, we can feasibly adapt the Ag/AgCl electrode to various bioelectronic devices and utilize it to selectively control $[Cl^-]$ in solution with V_{Cl^-} . Here, we design a chloride modulator, which transfers Cl^- from a reservoir electrolyte with a rich Cl^- source to a target electrolyte under control. The Ag/AgCl NPs act as the working electrode. The selectivity of AgCl to Cl^- ensures it a storage media specifically to Cl^- and allows Cl^- to move between reservoir and target depending on V_{Cl^-} . Thus, the chloride modulator can manipulate $[Cl^-]$ in a much more extensive range than a single Ag/AgCl contact. As proof-of-concept, we culture cells in the target chamber and study the effect of $[Cl^-]$ modulation on their function.

Figure 3(a) shows the schematic of the chloride modulator (side view), and the design is similar to previously reported proton modulator with Pd/PdH_x electrodes.¹⁹ The chloride modulator is composed of two independent chambers, referred to as reservoir (left) and target (right), respectively, connected by an anion exchange membrane (AEM). Figure 3(b) shows the optical image of the device. The reservoir has 0.1M KCl to provide a rich Cl^- source, and we change $[Cl^-]$ of the target solution, which can contain 100 μ M MQAE in de-ionized (DI) water [Fig. 3(c)], or cells [Figs. 3(d) and 3(e)]. We use an Ag/AgCl NPs microelectrode as the working electrodes, providing multiple independent openings for Cl^- to enter/leave the target solution. Here, we define the potential difference between the Ag/AgCl and Pt electrode in the reservoir as $V_{Cl^-,R}$, and the potential difference between the Ag/AgCl and Pt electrode in the target as V_{Cl^-} . AEM is a polymer with high conductivity for anions due to their large amount of fixed cationic groups that support the storage and transport of mobile anions through the membrane, and its exclusion to cations ensures that the majority of measured currents are from the moving of anions.⁴³ Here, AEM is a mixture of polyvinyl alcohol (PVA) and poly(diallyldimethylammonium chloride) (PDMA), which work

as the hydrophilic matrix and polycation, respectively. To avoid the undesirable passive diffusion current caused by the $[Cl^-]$ gradient between the reservoir and target, we pattern a thin cation exchange membrane (CEM), PVA and polystyrene sulfate acid (PSS) mixture, at the opening of the MEAs to form a Donnan exclusion barrier. The AEM and CEM function together to provide a bridge that allows for an electrophoretic Cl^- flow during stimulation with a voltage across the bridge and minimization of passive diffusion current. More details about device fabrication are shown in Fig. S5.

We design a 4-step process in Table I to control $[Cl^-]$ in target solution periodically by driving Cl^- from and back to the reservoir, which results in the $[Cl^-]$ changes shown in Fig. 3(c). The Cl^- modulator also achieves diffusion limited spatial resolution with larger $[Cl^-]$ changes occurring close to the contacts that are active, with little or no $[Cl^-]$ changes observed in the non-active region (Fig. S6).

As a proof-of-concept, we used the chloride modulator to study the effects of extracellular $[Cl^-]$ on human pluripotent mamalian stem cells (hiPSCs) and their V_{mem} [Figs. 3(d) and 3(e)]. A cell's resting potential, V_{mem} , is an electrical control signal that occurs between the inside of the cell and the extracellular environment.⁴⁴ V_{mem} affects cell physiology and functions such as proliferation, differentiation, migration, and apoptosis, as well as cell-cell communication and large-scale morphogenesis.⁴⁵

Chloride is the major anion in extracellular environments. In hiPSCs, an increase in extracellular $[Cl^-]$ results in cell hyperpolarization (higher V_{mem}), and a decrease in extracellular $[Cl^-]$ results in cell depolarization (lower V_{mem}).⁴⁶ We measure V_{mem} of the hiPSCs using ArcLight, a fluorescent reporter that we expressed on the cell membrane, whose fluorescence intensity increases when V_{mem} increases.⁴⁷ By switching the environment between high $[Cl^-]$ and low $[Cl^-]$ conditions using the same protocol in Table I, we observe that V_{mem} of hiPSCs shifts with the expected pattern as measured by the ArcLight fluorescence intensity [Fig. 3(d)]. Figure 3(e) shows the fluorescence images of the cells at $t = 75$ s and $t = 119$ s, corresponding to high (hyperpolarized) and low V_{mem} (depolarized), respectively. This change in fluorescence occurs close to the activated area and not far away from the active electrodes, indicating that the induced change in $[Cl^-]$ is responsible for the measured V_{mem} change. While this is a proof-of-concept, it shows how the Cl^- modulator is able to affect the cell function.

TABLE I. 4-step process that modulates $[Cl^-]$ in the target solution.

	Step	$V_{Cl^-,R}$ (V)	V_{Cl^-} (V)	Time (s)	$[Cl^-]$
1	Transfer Cl^- from reservoir to AgCl	2	0	5	High
2	AgCl release Cl^- to target	0	-1.5	30	High
3	Remove Cl^- from AgCl to reservoir	-1	0	5	Low
4	AgCl absorb Cl^- from target	0	1	10	Low

V. CONCLUSION

Ag/AgCl is a well-known reference electrode that has been used in electrochemistry for decades. Here, we first demonstrate Ag/AgCl as a Cl^- transducer that controls $[\text{Cl}^-]$ by transferring Cl^- from and to solution controlled by an applied voltage, V_{Cl^-} . Furthermore, we investigate kinetics of the conversion between Ag/AgCl by using electrochemical techniques, which are consistent with Cl^-/e^- transformation and critical for controlling $[\text{Cl}^-]$ by electronic means. This control paves the way to the integration of Ag/AgCl into complex bioelectronic devices for dynamic control of bioelectric signaling *in vivo* and *in vitro* models of physiology and morphogenesis. As a proof of concept, we adapt Ag/AgCl into a chloride modulator that precisely regulates $[\text{Cl}^-]$ in solution and affects the membrane voltage of pluripotent stem cells. Since Cl^- is a critical anion in bioelectricity, the accurate regulation of $[\text{Cl}^-]$ is currently in high demand and has potential in bioelectronic therapies.

SUPPLEMENTARY MATERIAL

See the [supplementary material](#) for the fluorescence dye calibration, Ag/AgCl NP electroplating, and fabrication of the chloride modulator.

ACKNOWLEDGMENTS

This research was sponsored by the Defense Advanced Research Projects Agency (DARPA), Army Research Office, under Cooperative Agreement No. W911NF-18-2-0104, and the Department of Interior, Award No. D20AC00003. The content of the information does not necessarily reflect the position or the policy of the Government, and no official endorsement should be inferred. Microfabrication was performed using equipment sponsored by the W. M. Keck Center for Nanoscale Optofluidics, the California Institute for Quantitative Biosciences (QB3), and the Army Research Office, Award No. W911NF-17-1-0460. We also acknowledge Dr. Tom Yuzvinsky for the help in performing electron microscopy and the W. M. Keck Center for Nanoscale Optofluidics for the use of the FEI Quanta 3D Dualbeam microscope.

DATA AVAILABILITY

The data that support the findings of this study are available from the corresponding author upon reasonable request.

REFERENCES

- D. S. Adams, A. Masi, and M. Levin, *Development* **134**(7), 1323–1335 (2007).
- M. Levin, J. Selberg, and M. Rolandi, *iScience* **22**, 519 (2019).
- J. Leger, M. Berggren, and S. Carter, *Iontronics: Ionic Carriers in Organic Electronic Materials and Devices* (CRC Press, 2016).
- G. Tarabella, F. M. Mohammadi, N. Coppède, F. Barbero, S. Iannotta, C. Santato, and F. Cicoira, *Chem. Sci.* **4**(4), 1395–1409 (2013).
- M. Jia and M. Rolandi, *Adv. Healthcare Mater.* **9**(5), 1901372 (2020).
- H. Yuk, B. Lu, and X. Zhao, *Chem. Soc. Rev.* **48**(6), 1642–1667 (2019).
- J. Selberg, M. Gomez, and M. Rolandi, *Cell Syst.* **7**(3), 231–244 (2018).
- M. Nishizawa, *Bull. Chem. Soc. Jpn.* **91**(7), 1141–1149 (2018).
- J. Isaksson, P. Kjäll, D. Nilsson, N. Robinson, M. Berggren, and A. Richter-Dahlfors, *Nat. Mater.* **6**(9), 673–679 (2007).
- A. Williamson, J. Rivnay, L. Kergoat, A. Jonsson, S. Inal, I. Uguz, M. Ferro, A. Ivanov, T. A. Sjöström, and D. T. Simon, *Adv. Mater.* **27**(20), 3138–3144 (2015).
- A. Jonsson, Z. Song, D. Nilsson, B. A. Meyerson, D. T. Simon, B. Linderöth, and M. Berggren, *Sci. Adv.* **1**(4), e1500039 (2015).
- C. Zhong, Y. Deng, A. F. Roudsari, A. Kapetanovic, M. Anantram, and M. Rolandi, *Nat. Commun.* **2**(1), 476 (2011).
- E. E. Josberger, Y. Deng, W. Sun, R. Kautz, and M. Rolandi, *Adv. Mater.* **26**(29), 4986–4990 (2014).
- T. Miyake, E. E. Josberger, S. Keene, Y. Deng, and M. Rolandi, *APL Mater.* **3**(1), 014906 (2015).
- Z. Hemmatian, S. Keene, E. Josberger, T. Miyake, C. Arboleda, J. Soto-Rodríguez, F. Baneyx, and M. Rolandi, *Nat. Commun.* **7**(1), 12981 (2016).
- T. Jiang, A. Hall, M. Eres, Z. Hemmatian, B. Qiao, Y. Zhou, Z. Ruan, A. D. Couse, W. T. Heller, and H. Huang, *Nature* **577**(7789), 216–220 (2020).
- Z. Hemmatian, R. H. Tunuguntla, A. Noy, and M. Rolandi, *PLoS One* **14**(2), e0212197 (2019).
- J. Soto-Rodríguez, Z. Hemmatian, E. E. Josberger, M. Rolandi, and F. Baneyx, *Adv. Mater.* **28**(31), 6581–6585 (2016).
- X. Strakosas, J. Selberg, X. Zhang, N. Christie, P. H. Hsu, A. Almutairi, and M. Rolandi, *Adv. Sci.* **6**(7), 1800935 (2019).
- Z. Hemmatian, E. Jalilian, S. Lee, X. Strakosas, A. Khademhosseini, A. Almutairi, S. R. Shin, and M. Rolandi, *ACS Appl. Mater. Interfaces* **10**(26), 21782–21787 (2018).
- M. Amit, S. Roy, Y. Deng, E. Josberger, M. Rolandi, and N. Ashkenasy, *ACS Appl. Mater. Interfaces* **10**(2), 1933–1938 (2018).
- N. Yunos, R. Bellomo, D. Story, and J. Kellum, *Crit. Care* **14**(4), 226 (2010).
- V. A. T. Dam, M. A. G. Zevenbergen, and R. Van Schaijk, *Procedia Eng.* **120**, 237–240 (2015).
- P. White and M. R. Broadley, *Ann. Bot.* **88**(6), 967–988 (2001).
- D. Arosio and G. M. Ratto, *Front. Cell. Neurosci.* **8**, 258 (2014).
- A. L. Hodgkin and P. Horowitz, *J. Phys.* **148**(1), 127 (1959).
- D. Blackiston, D. S. Adams, J. M. Lemire, M. Lobikin, and M. Levin, *Dis. Models Mech.* **4**(1), 67–85 (2011).
- D. J. Blackiston, G. M. Anderson, N. Rahman, C. Bieck, and M. Levin, *Neurotherapeutics* **12**(1), 170–184 (2015).
- G. J. Janz and D. J. G. Ives, *Ann. N. Y. Acad. Sci.* **148**(1), 210–221 (1968).
- G. Inzelt, *Handbook of Reference Electrodes* (Springer, 2013), pp. 331–332.
- M. A. Climent-Llorca, E. Viqueira-Pérez, and M. M. López-Atalaya, *Cem. Concr. Res.* **26**(8), 1157–1161 (1996).
- F. Pargar, H. Kolev, D. A. Koleva, and K. van Breugel, *J. Mater. Sci.* **53**(10), 7527–7550 (2018).
- Y. Ikeuchi, H. Kogiso, S. Hosogi, S. Tanaka, C. Shimamoto, T. Inui, T. Nakahari, and Y. Marunaka, *J. Physiol. Sci.* **68**(2), 191–199 (2018).
- Y. Abbas, D. B. de Graaf, W. Olthuis, and A. van den Berg, *Anal. Chim. Acta* **821**, 81–88 (2014).
- J. Peng, Y. Deng, D. Wang, X. Jin, and G. Z. Chen, *J. Electroanal. Chem.* **627**(1–2), 28–40 (2009).
- I.-Y. Huang, R.-S. Huang, and L.-H. Lo, *Sens. Actuators, B* **94**(1), 53–64 (2003).
- G. Tarabella, C. Santato, S. Y. Yang, S. Iannotta, G. G. Malliaras, and F. Cicoira, *Appl. Phys. Lett.* **97**(12), 205 (2010).
- Y. Deng, D. Wang, W. Xiao, X. Jin, X. Hu, and G. Z. Chen, *J. Phys. Chem. B* **109**(29), 14043–14051 (2005).
- B. J. Polk, A. Stelzenmüller, G. Mijares, W. MacCrehan, and M. Gaitan, *Sens. Actuators, B* **114**(1), 239–247 (2006).
- N. Elgrishi, K. J. Rountree, B. D. McCarthy, E. S. Rountree, T. T. Eisenhart, and J. L. Dempsey, *J. Chem. Educ.* **95**(2), 197–206 (2018).
- J.-M. Savéant, *Elements of Molecular and Biomolecular Electrochemistry* (Wiley-VCH, New Jersey, 2006).

⁴²A. J. Bard and L. R. Faulkner, *Electrochem. Methods* **2**(482), 580–632 (2001).

⁴³N. Berezina, N. Kononenko, O. Dyomina, and N. Gnusin, *Adv. Colloid Interface Sci.* **139**(1-2), 3–28 (2008).

⁴⁴J. L. Whited and M. Levin, *Curr. Opin. Genet. Dev.* **57**, 61–69 (2019).

⁴⁵M. Levin, G. Pezzulo, and J. M. Finkelstein, *Annu. Rev. Biomed. Eng.* **19**, 353–387 (2017).

⁴⁶A. Shiozaki, E. Otsuji, and Y. Marunaka, *World J. Gastrointest. Oncol.* **3**(8), 119 (2011).

⁴⁷Y. Xu, P. Zou, and A. E. Cohen, *Curr. Opin. Chem. Biol.* **39**, 1–10 (2017).